Kinetics of passivation of a nickel-base alloy in high temperature water

A. Machet[1,2], A. Galtayries[1*], S. Zanna[1], P. Jolivet[2],
M. Foucault[3], P. Combrade[3], P. Scott[2], P. Marcus[1*]

[1] *Laboratoire de Physico-Chimie des Surfaces, CNRS-ENSCP (UMR 7045), Ecole Nationale Supérieure de Chimie de Paris, Université Pierre et Marie Curie, F-75231 Paris cedex 05*

[2] *Framatome ANP, Tour AREVA, F-92084 Paris-la-Défense*

[3] *Framatome ANP, Centre Technique, F-71205 Le Creusot*

Abstract

The kinetics of passivation and the composition of the surface oxide layer, in high temperature and high pressure water, of a nickel-chromium-iron alloy (Alloy 600) have been investigated by X-ray Photoelectron Spectroscopy (XPS). The samples have been exposed for short (0.4 – 8.2 min) and longer (0 – 400 hours) time periods to high temperature (325°C) and high pressure water (containing boron and lithium) under controlled hydrogen pressure. The experiments were performed in two types of autoclaves : a novel autoclave dedicated to short time periods and a classic static autoclave for the longer exposures.
In the initial stage of passivation, a continuous ultra-thin layer of chromium oxide (Cr_2O_3) is rapidly formed on the surface with an external layer of chromium hydroxide.
For longer times of passivation, the oxide layer is in a duplex form with an internal chromium oxide layer and an external layer of nickel hydroxide.
The growth of the internal Cr_2O_3 oxide layer has been fitted by three classical models (parabolic, logarithmic and inverse logarithmic laws) for the short passivation times, and the growth curves have been extrapolated to longer passivation periods. The comparison with the experimental results reveals that the kinetics of passivation of Alloy 600 in high temperature and high pressure water, for passivation times up to 400 hours, is well fitted by a logarithmic growth law.

Keywords : Alloy 600 ; passivation ; X-ray Photoelectron Spectroscopy (XPS) ; high temperature, high pressure water ; PWR ; kinetics.

* Corresponding authors : anouk-galtayries@enscp.jussieu.fr, philippe-marcus@enscp.jussieu.fr
Fax: + 33 1 46 34 07 53

Introduction

The oxidation behaviour of nickel base alloys in high temperature and high pressure water, simulating the primary circuit of steam generators (SG) of pressurised water reactors (PWR), has been studied by several authors [1-12]. It is generally recognised that the passivity of this alloy in such conditions is due to the formation of a chromium-rich oxide layer which provides a diffusion barrier and reduces the corrosion rate. In this context, as a consequence, the passive layer reduces the release of corrosion products, such as nickel cations, in primary side water. It is of crucial importance because of the activation of ^{58}Ni into ^{58}Co in the primary circuit, which increases the global radioactivity of the primary circuit of PWRs. For safety reason for the maintenance staff, it is very important to control and limit the release of nickel species in the primary circuit. Another important application of a better knowledge of the formation of the passive film is the understanding of stress corrosion cracking mechanisms [13]. Very few papers deal with the initial stages of passivation in high temperature and high pressure water. The aim of this work was to identify the nature of the oxide layer by X-ray Photoelectron Spectroscopy (XPS), from very short to longer times of passivation of Alloy 600 and to determine the kinetic law for the growth of the barrier oxide layer for both short and longer times.

Experimental

Materials

Polycrystalline samples of commercial Alloy 600 (Ni-16Cr-9Fe (weight %) or Ni-18Cr-9Fe (atomic %)) were cut into disks of 15 mm diameter and 1 mm thickness. The polycrystalline coupons were mechanically polished to a 1 µm diamond finish. Prior to the short passivation time periods, further cleaning was performed, in UHV conditions, in the XPS spectrometer, with argon ion sputtering (4 kV, 0,9 µA, $1x10^{-4}$ Pa ($1x10^{-6}$ mbar), 60 minutes).

Passivation

The short passivation times in high temperature, high pressure water (325°C, ~155 bar) were performed in a titanium microautoclave, dedicated to short times of treatment (a few tens of seconds and up), allowing transfers of the samples to and from the XPS spectrometer without air exposure. The cooling in the microautoclave is rapid (~2 minutes) and is performed under argon, as well as the transfer to the XPS, so that the possible changes of the surface composition are minimised. The longer passivation times (up to 400 hours) were performed in a static autoclave, and the samples were rinced, dried and transferred in air before XPS analysis.

In both systems, the aqueous solution simulating unsaturated PWR primary water conditions contained 2 $mg.l^{-1}$ Li and 1200 $mg.l^{-1}$ B. A hydrogen overpressure of 0.3 bar was maintained to ensure a dissolved H_2 concentration of 35 $cm^3.kg^{-1}$ and a low oxygen content of <30 $\mu g.kg^{-1}$. In our experimental conditions, the pH of the solution was 7.1 and the potential was -0.808 V/SHE. This potential is calculated from the H_2/H^+ equilibrium potential, close to the corrosion potential of Alloy 600 [14].

Surface Analysis

For the surface characterisation by XPS, the Ni 2p, Cr 2p, Fe 2p, O 1s, C 1s, B 1s and Li 1s core level spectra were recorded with a VG ESCALAB Mk II X-ray photoelectron spectrometer, with a AlK_α or MgK_α radiation ($h\nu$=1486.6 and 1253.6 eV, respectively), at a pass energy of 20 eV. The spectrometer was calibrated against the reference binding energies (BEs) of clean Ni and Au samples (Ni $2p_{3/2}$ and Au $4f_{7/2}$ lines set at 852.8 eV and 84.0 eV,

respectively). The take-off angles of the photoelectrons were 90° and 45°, with respect to the sample surface. In the XPS spectrometer, the base pressure of the analysis chamber was 3x 10^{-10} Torr. The argon ions sputtering used to clean the surface prior to passivation was carried out in the analysis chamber with an ion energy of 3 keV. To analyse the individual contributions of the Ni $2p_{3/2}$, Cr $2p_{3/2}$, Fe $2p_{3/2}$, O 1s, C 1s, and B 1s core levels, peak decomposition was carried out with a commercial computer program (Eclipse provided by VG) using Gaussian/Lorentzian peak shapes, and a Shirley background. For longer passivation times, the depth profile mode was used, with 3 keV argon ions, a target current of 2.5 µA.cm^{-2}, and an Ar pressure of 1x10^{-4} Pa (1x10^{-6} mbar).

Results

Short oxidation times

Figure 1 (a) shows the Cr $2p_{3/2}$ core level spectra recorded after passivation of the polycrystalline alloy for three different time periods: 0.4 min, 1.2 min and 8.2 min. The Cr $2p_{3/2}$ peaks have been systematically decomposed into up to three components: one located at a binding energy (BE) of 574.3±0.1 eV, and two other ones located at BEs of 577.2±0.5 eV and 577.9±0.1 eV. By comparison with published data [15-17], the signal at 574.3 eV is assigned to metallic chromium in the nickel-base alloy, the signal at 577.2 eV to Cr^{3+} in Cr_2O_3 [1,15,18] and the signal at 577.9 to Cr^{3+} in $Cr(OH)_3$ [1,15]. With increasing exposure time, the intensity of metallic chromium decreases, but the signal is still present after 8 minutes of passivation. The signal of chromium hydroxide disappears, between 1.2 and 8.2 min, in favour of chromium oxide.

For the Ni $2p_{3/2}$ peak decomposition (Figure 1 (b)), two main components (and the associated satellites) are considered: a signal from metallic nickel in the alloy at a BE of 853.1±0.1 eV, and another feature located at a BE of 856.8±0.4 eV. The latter signal is attributed to $Ni(OH)_2$ on the surface. The absence of Ni^{2+} signal corresponding to NiO in the Ni 2p core level spectra, whatever the passivation time, is in agreement with the Pourbaix diagram of Ni at 300°C [19,20], showing that NiO is not stable in the experimental E-pH conditions of this work. The signal from metallic nickel is dominant for 0.4 and 1.2 min of passivation. After 8 minutes the metallic signal is still present but the signal from nickel hydroxide has become significantly more intense.

Both core level spectra of Cr and Ni indicate the growth of a surface oxide layer (composed of oxide and hydroxides). The Fe $2p_{3/2}$ spectra (not shown here) show low intensity signals, due to the low concentration of iron in the alloy as well as on the surface after passivation (the surface concentration in the oxide layer is <5 at. %).

The peak decompositions of the alloying elements are well correlated with the O 1s peak decomposition (Figure 1 (c) for 1.2 and 8.2 min), including the chromium oxide feature at a BE of 531.1±0.6 eV, the chromium hydroxide feature at a BE of 531.8±0.2 eV (corresponding to 0.4 and 1.2 min in Figure 1) and a feature at 532.2±0.5 eV attributed to the hydroxide ions in nickel hydroxide. As a minor feature, one can systematically see a small oxygen signal of O^{2-} in Fe_2O_3 (530.6±0.3 eV) and, in the case of 1.2 min of passivation, an additional oxygen signal attributed to adsorbed water (532.4±0.4 eV).

Figure 1 (c) shows the angle-dependent XPS data (90° and 45°) for the O 1s core level and the peak decomposition, after a passivation time of 8.2 min in the microautoclave. The main difference in the relative intensities, at 90° and 45°, of the components attributed to $Ni(OH)_2$ (BE of 532.5±0.1 eV) and to Cr_2O_3 (BE of 531.2±0.1 eV) is the higher intensity of the hydroxyl groups, with respect to the intensity of oxygen in oxide, at the more grazing take-off angle. This result shows that the nickel hydroxide is located on the chromium oxide surface. A simple layer model, based on the stratification of the passive layer, is shown in Figure 2.

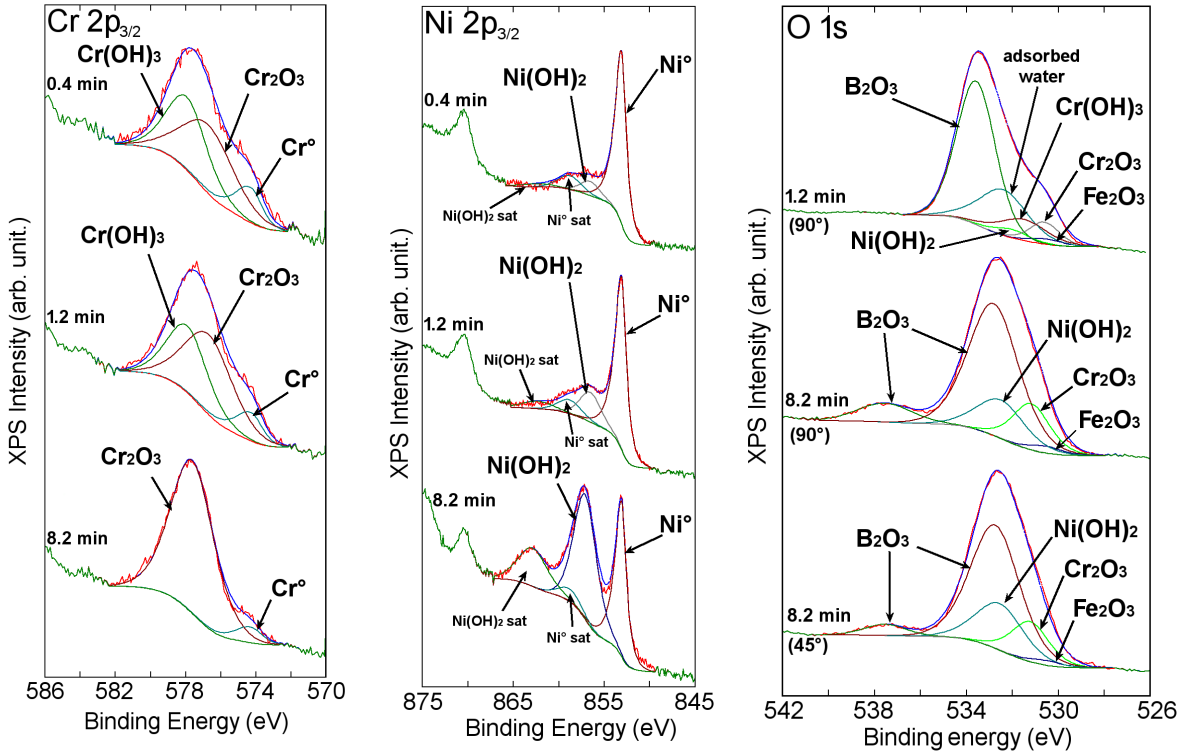

(a) (b) (c)

Figure 1: Cr $2p_{3/2}$ (a), Ni $2p_{3/2}$ (b) and O 1s (c) core level spectra (and the peak fitting) of a Ni-16Cr-9Fe (wt. %) alloy (Ni-18Cr-9Fe at. %) after different passivation times in the microautoclave, in high temperature (325°C) water (MgK_α X-ray source, take-off angle of 90° or otherwise indicated).

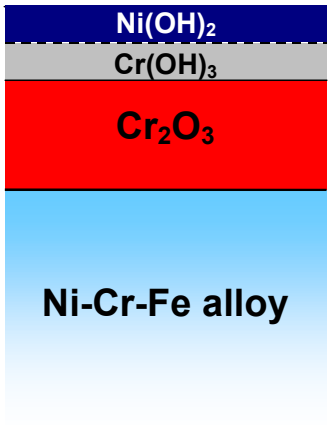

Figure 2: Layer model used for the calculation of the thickness of the different layers present in the passive film formed on the Ni-16Cr-9Fe (wt. %) (Ni-18Cr-9Fe at. %) alloy surface after oxidation in high temperature (325°C) water.

It consists of an outermost layer of $Ni(OH)_2$, an intermediate layer of $Cr(OH)_3$ and an inner Cr_2O_3 oxide layer, in contact with the alloy. Due to its low concentration (< 5 at.%), and to the difficulty to locate the small amount of detected Fe_2O_3, it was not included in this model.
The equivalent thickness of the external layer ($Cr(OH)_3$ and $Ni(OH)_2$) and the Cr_2O_3 internal layer has been systematically determined from the XPS intensities of the metallic and oxide features. Figure 3 displays the results corresponding to the Cr_2O_3 inner layer, plotted as a function of passivation time. From the examination of Figure 3, three domains are observed :

(i) after the first exposure (0.4 min), the formation of chromium oxide,

(ii) from 0.4 to ~4 min, there is a plateau corresponding to a Cr_2O_3 oxide layer of about 1 nm.

(iii) beyond ~4 min, a re-oxidation is observed, with the growth of the Cr_2O_3 layer.

The three domains are indicated on Figure 3.
After 8 minutes of passivation, the oxide layer is still growing, exhibiting a duplex layer with islands of $Ni(OH)_2$ on top of the continuous inner layer of Cr_2O_3 (2 nm thick). Complementary information on the structural aspects of the inner Cr_2O_3 layer have been obtained by Scanning Tunneling Microscopy (STM), indicating that this layer is crystalline and that its structure is consistent with the hexagonal structure of the oxygen sub-lattice in the (0001) orientation of α-Cr_2O_3 [21].

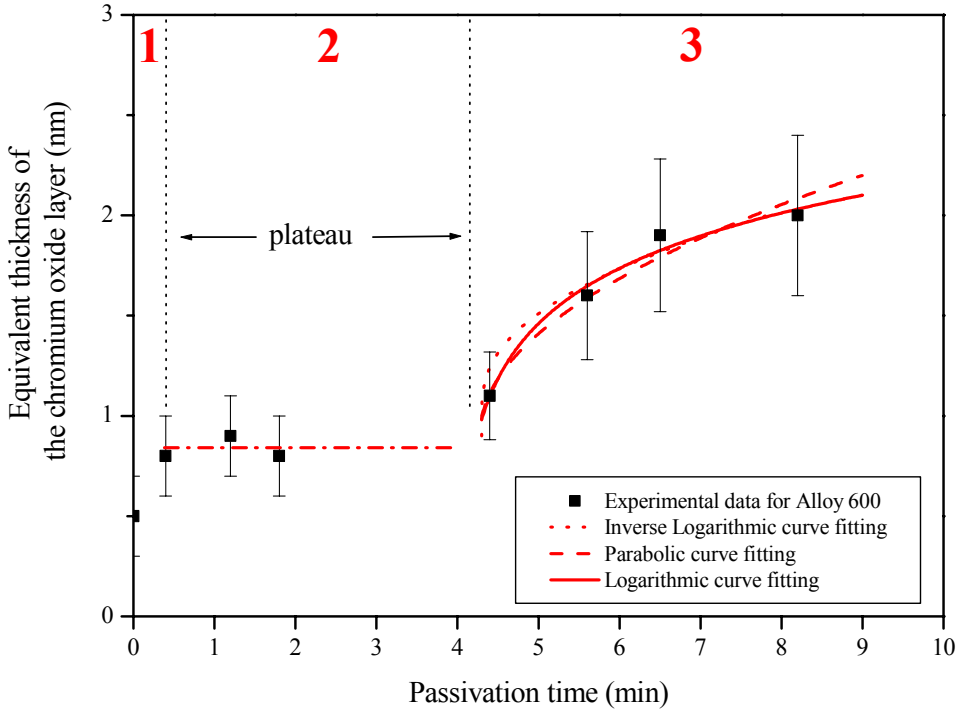

Figure 3: Equivalent thickness of the Cr_2O_3 internal layer formed on a Ni-16Cr-9Fe (wt. %) alloy (Ni-18Cr-9Fe at. %) as a function of passivation time in the microautoclave, and the parabolic, logarithmic and inverse logarithmic fitting of the growth of the Cr_2O_3 layer in Step 3.

Figure 3 displays the curve fitting of the kinetics of the Cr_2O_3 growth by three classical kinetic models: parabolic, logarithmic and inverse logarithmic, the equations of which being:

- parabolic fitting: $(d_{Cr_2O_3} - 0.9)^2 = 0.35 \cdot (t - 4.3)$
- logarithmic fitting: $d_{Cr_2O_3} = 0.9 + 0.39 \cdot \ln(4.06 \cdot (t - 4.3) + 1)$
- inverse logarithmic fitting: $\frac{0.6}{\left(d_{Cr_2O_3} - 0.9\right)} = 1.62 - \ln \frac{t - 4.3}{\left(d_{Cr_2O_3} - 0.9\right)^2}$

At this point, it is not possible to discriminate between the three growth laws, but it will be shown below that the discrimination becomes possible by extrapolating to long exposure times and comparing with the experimental data.

Longer oxidation times

The samples have been exposed from 0 (blank test) to 400 hours in high temperature (325°C) and high pressure water in a static autoclave. The XPS spectra of the oxidised samples show that the signals corresponding to the metallic alloy (Ni, Cr, Fe) are not detected, which indicates that the oxide layer is thicker than the one measured for short oxidation times. XPS depth profiles were performed in order to get in-depth information on the composition of the oxide layer. Figure 4 displays one example of the XPS profiles obtained on the Ni-16Cr-9Fe (wt. %) alloy (Ni-18Cr-9Fe at. %) oxidised 100 hours in high temperature water, as a function of sputtering time.

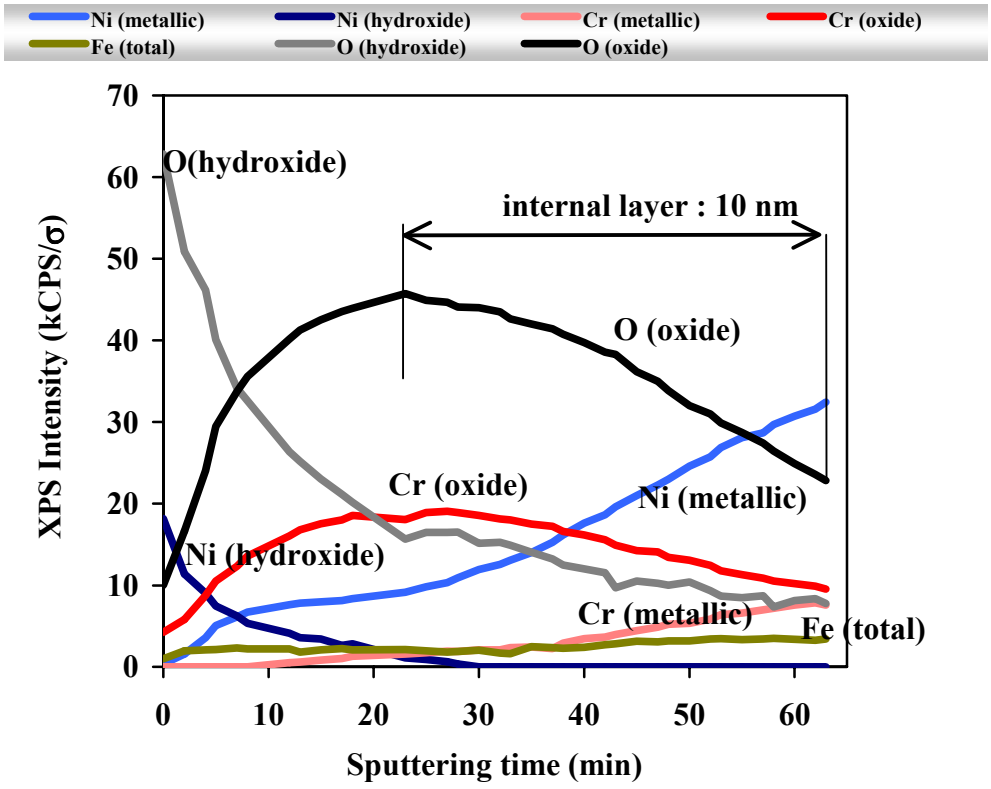

Figure 4: XPS depth profile of the oxide layer formed on a Ni-16Cr-9Fe (wt. %) alloy (Ni-18Cr-9Fe at. %) after 100 hours in high temperature (325°C) water, in a static autoclave (AlK_α X-ray source, sputtering conditions: Ar ions, 3 keV, 2.5 µA.cm^{-2}).

To be consistent with the results obtained for short times of oxidation, after sputtering the Ni $2p_{3/2}$ core level was systematically decomposed into metallic nickel from the alloy (853.1 eV) and $Ni(OH)_2$ (857.3 eV), the Cr $2p_{3/2}$ into metallic chromium from the alloy (574.4 eV) and Cr_2O_3 (577.4 eV). The intensity of the Fe 2p core level was very weak so the peak decomposition was difficult to perform into metallic and oxidised components, and only the total intensity of the Fe 2p core level peak is reported in Figure 4. As regards the O 1s core level peak, it was decomposed into two constituents: the hydroxyl (OH^- at 532.8±0.2 eV) and the oxygen in oxide (O^{2-} at 531.1±0.2 eV).
From the examination of Figure 4, one can observe that both the intensities corresponding to the hydroxyl contributions in O 1s and Ni 2p core levels decrease rapidly as a function of sputtering time. At the same time, an increase of the oxide contributions in the O 1s and Cr $2p_{3/2}$ core levels is observed. It is concluded that the external layer is mainly composed of $Ni(OH)_2$ while the inner layer is composed of Cr_2O_3. The weak intensity of the signal of the Fe $2p_{3/2}$ core level does not present any significant variation during sputtering.
In order to determine the thickness of the chromium oxide inner layer from the XPS profiles, we have used the intensity of oxygen in the oxide (O^{2-}). The sputtering time between the maximum of the intensity (when the chromium oxide is reached), and the intensity at half maximum (assigned to the oxide/alloy interface) is measured. The sputtering time is then converted into thickness, using the calibration obtained from Nuclear Reaction Analysis (NRA): 0.25 $nm.min^{-1}$ for a target current of 2.5 $\mu A.cm^{-2}$ [22].
After oxidation of Alloy 600, for 100 hours in high temperature water (Figure 4), the equivalent thickness of Cr_2O_3 is 10 nm ±1 nm. The same systematic treatment of the XPS depth profiles, after oxidation times from 0 (blank test) to 400 hours, has allowed us to obtain the thickness of Cr_2O_3 for each passivation time. Figure 5 shows the kinetics of chromium oxide growth for passivation times up to 400 hours. The thickness of the inner Cr_2O_3 layer increases significantly up to 20 hours, then it becomes almost constant.

Extrapolation of the growth laws calculated for short oxidation times and comparison with the experimental data

In order to relate the data of the kinetics of passivation of the alloy for short and long oxidation times (up to 400 hours), the three kinetic laws fitting the data for the short oxidation times have been extrapolated, using the initial value of the Cr_2O_3 oxide layer (measured after the blank test). The three equations are now :

- parabolic fitting: $(d_{Cr_2O_3} - 6)^2 = 0{,}35 \cdot t$
- logarithmic fitting: $d_{Cr_2O_3} = 6 + 0{,}39 \cdot \ln(4{,}06 \cdot t + 1)$
- inverse logarithmic fitting: $\dfrac{0.6}{\left(d_{Cr_2O_3} - 6\right)} = 1.62 - \ln \dfrac{t}{\left(d_{Cr_2O_3} - 6\right)^2}$

The three corresponding curves are plotted on Figure 5. It comes from the comparison of the fitted and experimental data that the parabolic and inverse logarithmic laws are out of range, while a satisfactory agreement is obtained with the logarithmic law.

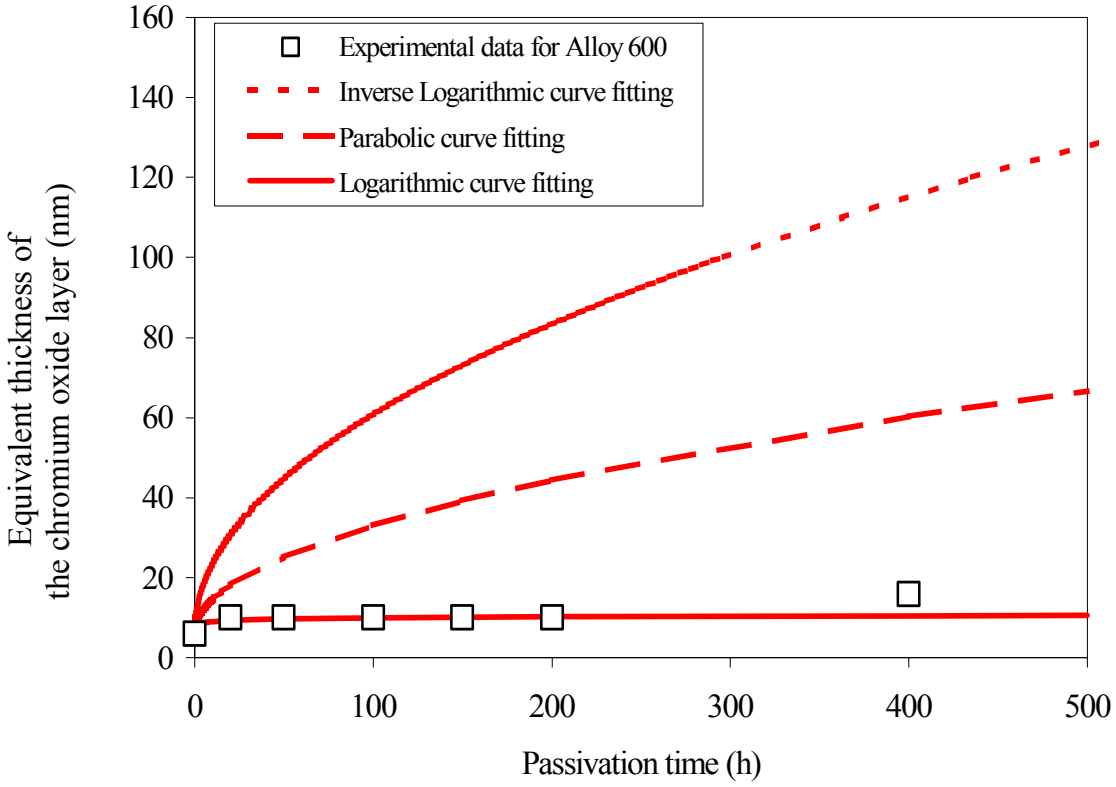

Figure 5: Kinetics of passivation of a Ni-16Cr-9Fe (wt. %) alloy (Ni-18Cr-9Fe at. %) in high temperature (325°C) water: thickness of the inner Cr_2O_3 layer vs. passivation time. Three extrapolations from the data obtained for short oxidation times are proposed: parabolic, logarithmic and inverse logarithmic models.

Discussion

In the initial stage of oxidation, the mechanisms of passivation of the Ni-16Cr-9Fe (wt. %) alloy (Ni-18Cr-9Fe at. %) involve three steps:

- Step 1: selective dissolution of nickel from the metallic alloy, and nucleation and growth of Cr_2O_3 islands, covered by $Cr(OH)_3$, in contact with the primary water solution,
- Step 2: coalescence of the Cr_2O_3 islands and formation of a continuous layer of Cr_2O_3 (about 1 nm thick), with an outer layer of $Cr(OH)_3$. At this point, there is a temporary blocking of the growth of Cr_2O_3, evidenced by the plateau in the kinetics of Figure 3,
- Step 3: the oxide growth starts again with the conversion of $Cr(OH)_3$ into Cr_2O_3 according to: $Cr(OH)_3 + Cr \rightarrow Cr_2O_3 + 3\ H^+ + 3\ e^-$ and then the further growth of Cr_2O_3.

To check the consistency of this mechanism, the growth of Cr_2O_3 has been followed from the depth profiles obtained for longer oxidation times.

The comparison of the extrapolated growth law to longer times shows that in the range of passivation times up to 400 hours, it is possible to rule out unambiguously the parabolic and inverse logarithmic laws. Only the logarithmic law fits well the experimental data. From a mechanistic point of view, the fact that the parabolic law does not fit the data shows that the hypothesis of thermally activated solid state diffusion is not valid here. The mechanism associated to a logarithmic law involves the mobility of ions in a high field (with the tunneling of electrons through the oxide). However, the thickness of 10 nm, obtained here for

the Cr_2O_3 oxide layer, seems too large for the electron tunneling effect. However, one has to remember that the chromium oxide is crystalline and grain boundaries are present in the oxide layer [21]. Such defects, and possibly other defects, can allow the transfer of electrons.
This approach has revealed that it is possible to follow the kinetics of the growth of the inner Cr_2O_3 layer in the initial stages of passivation. It is the first direct evidence of the key role of short oxidation times in the kinetics of the Cr_2O_3 oxide growth on nickel-base alloys in high temperature water.

Conclusions

The kinetics of passivation in high temperature and high pressure water of a Ni-16Cr-9Fe (wt. %) alloy (Ni-18Cr-9Fe at. %) has been investigated. The composition and the thickness of the surface oxide layer have been measured for very short oxidation times (minutes) and longer oxidation times (up to 400 hours). The thickness of the inner chromium oxide barrier layer has been measured as a function of oxidation times. From the three kinetic laws that fit well the experimental data for the short oxidation times, only the logarithmic law can be retained from the comparison of the extrapolated growth laws with the experimental data for long oxidation times. The logarithmic law is characteristic of an apparent mechanism of high charge field effect for the growth of the internal Cr_2O_3 layer.

References

1. J. E. Castle, C. R. Clayton, Passivity of Metals, R. P. Frankenthal and J. Kruger Eds., The Electrochemical Society, Princeton, N. J., USA, p. 714 (1978).

2. N. S. McIntyre, D. G. Zetaruk, D. Owen, *J. Electrochem. Soc.,* **126,** 750 (1979).

3. C. Y. Chao, L. F. Lin, D. D. Macdonald, *J. Electrochem. Soc*., **128**, 1187 (1981).

4. L. F. Lin, C. Y. Chao, D. D. Macdonald, *J. Electrochem. Soc*., **128**, 1194 (1981).

5. R. L. Tapping, D. Davidson, E. McAlpine, D. H. Lister, *Corros. Sci*., **26**, 563 (1987).

6. P. Combrade, M. Foucault, D. Vançon, P. Marcus, J. M. Grimal, A. Gelpi, Proceedings of the 4th International Symposium on Environmental Degradation of Materials in Nuclear Power Systems-Water Reactors, D. Cubicciotti Ed., NACE, p. 79 (1989).

7. J. Robertson, *Corros. Sci*., **32**, 443 (1991).

8. T. M. Angeliu, G. S. Was, *J. Electrochem. Soc*., **140**, 1877 (1993).

9. N. Hakiki, D. Colin, O. De Bouvier, E. Picquenard, G. Sagon, J. Corset, M. Da Cunha Belo, Proceedings of the International Symp. Fontevraud III, Contribution of Materials Investigation to the Resolution of Problems Encountered in Pressurized Water Reactors, vol. 1, p. 327 (1994).

10. B. Stellwag, *Corros. Sci*., **40**, 337 (1998).

11. F. Carette, M. C. Lafont, G. Chataignier, L. Guinard, B. Pieraggi, *Surf. Interf. Anal*., **34**, 135 (2002).

12. F. Carette, L. Guinard, B. Pieraggi, Proceedings of the International Conference on Water Chemistry of Nuclear Reactor Systems, Operation Optimisation and New Developments (2002).

13 F. P. Ford and P. L. Andersen, in *Corrosion Mechanisms in Theory and Practice - Second Edition, Revised and Expanded*, Ed. P. Marcus, Marcel Dekker, Inc., New York (USA), (2002) and reference therein.

14. N. Totsuka, Z. Szklarska-Smialowska, *Corrosion*, **43**, 734 (1987).

15. P. Marcus, J. M. Grimal, *Corros. Sci*., **33**, 805 (1992).

16. V. Maurice, W. P. Yang, P. Marcus, *J. Electrochem. Soc.*, **141**, 3016 (1994).

17. A. M. Salvi, J. E. Castle, J. F. Watts, E. Desimoni, *Appl. Surf. Sci*., **90**, 333 (1995).

18. N. S. McIntyre, D. G. Zetaruk, D. Owen, *Appl. Surf. Sci*., **2**, 55 (1978).

19. B. Beverskog, I. Puigdomenech, *Corros. Sci.*, **39**, 969 (1997).

20. B. Beverskog, I. Puigdomenech, *Corros. Sci*., **39**, 43 (1997).

21. A. Machet, A. Galtayries, S. Zanna, L. Klein, V. Maurice, P. Jolivet, M. Foucault, P. Combrade, P. Scott, P. Marcus, *Electrochimica Acta*, **49**, 3957 (2004).

22. A. Machet, A. Galtayries, P. Marcus, A. Gelpi, C. Brun, P. Combrade, *J. Phys. IV*, **11**, Pr01-79 (2001).